PNAS RESEARCH ARTICLE | PHYSIOLOGY

A gain-of-function HCN4 mutant in the HCN domain is responsible for inappropriate sinus tachycardia in a Spanish family

Anabel Cámara-Checa[a,b,1], Francesca Perin[c,d,1], Marcos Rubio-Alarcón[a,b], María Dago[a,b], Teresa Crespo-García[a,b], Josu Rapún[a,b], María Marín[b], Jorge Cebrián[a,b], Ricardo Gómez[a,b], Francisco Bermúdez-Jiménez[c,d,e], Lorenzo Monserrat[b,f], Juan Tamargo[a], Ricardo Caballero[a,b,2,3], Juan Jiménez-Jáimez[c,d], and Eva Delpón[a,b,2]

Edited by Bruce Bean, Harvard Medical School, Boston, MA; received March 29, 2023; accepted October 12, 2023

In a family with inappropriate sinus tachycardia (IST), we identified a mutation (p.V240M) of the hyperpolarization-activated cyclic nucleotide–gated type 4 (HCN4) channel, which contributes to the pacemaker current (I_f) in human sinoatrial node cells. Here, we clinically study fifteen family members and functionally analyze the p.V240M variant. Macroscopic (I_{HCN4}) and single-channel currents were recorded using patch-clamp in cells expressing human native (WT) and/or p.V240M HCN4 channels. All p.V240M mutation carriers exhibited IST that was accompanied by cardiomyopathy in adults. I_{HCN4} generated by p.V240M channels either alone or in combination with WT was significantly greater than that generated by WT channels alone. The variant, which lies in the N-terminal HCN domain, increased the single-channel conductance and opening frequency and probability of HCN4 channels. Conversely, it did not modify the channel sensitivity for cAMP and ivabradine or the level of expression at the membrane. Treatment with ivabradine based on functional data reversed the IST and the cardiomyopathy of the carriers. In computer simulations, the p.V240M gain-of-function variant increases I_f and beating rate and thus explains the IST of the carriers. The results demonstrate the importance of the unique HCN domain in HCN4, which stabilizes the channels in the closed state.

HCN4 | single channel | HCN domain | inappropriate sinus tachycardia | mutation

Significance

Hyperpolarization-activated cyclic nucleotide–gated type 4 (HCN4) channels seem to contribute to the pacemaker current (I_f) in human sinoatrial node cells. They exhibit a unique N-terminal domain (HCND), which interacts with their C-terminal cyclic nucleotide–binding and voltage-sensor domains. HCND stabilizes the closed pore and regulates the membrane expression of HCN1-2 channels. In a family with inappropriate sinus tachycardia (IST), we identified a gain-of-function mutation (p.V240M) within the HCND. The variant increased the single-channel conductance and opening frequency and probability of HCN4 channels without modifying their sensitivity for cAMP and ivabradine or the membrane expression. Our results shed light on the understanding of the pathophysiology of IST and of the molecular determinants of the HCND of HCN4 channels.

Inappropriate sinus tachycardia (IST) is a clinical syndrome with an estimated prevalence of around 1% (more frequent in young women) and a significant impact on the quality of life of the affected individuals (1, 2). IST is defined by a sinus heart rate (HR) inexplicably higher than 100 beats per min (bpm) at rest or higher than 90 bpm on average over 24 h. The pathophysiology of IST is still not fully understood as the processes involved in pacemaking, and its modulation are extremely complex (1, 2). Any participating mechanisms can affect the HR and result in this syndrome, including an intrinsic increase in sinoatrial node automaticity (2), excess sympathetic tone and reduced cardiovagal tone (3), and circulating anti-beta-adrenergic receptor antibodies (4), among others.

The hyperpolarization-activated cyclic nucleotide–gated (HCN) channel family comprises 4 members (HCN1-4), and they have the peculiarity that they are activated by hyperpolarization rather than depolarization (5). These channels are expressed in the heart and in the central and peripheral nervous systems and exhibit a unique ion selectivity since they allow the passage of a depolarizing mixed Na^+ and K^+ current (5). In the heart, the current is known as pacemaker or funny current (I_f) (because of its quite unusual biophysical profile) and has a key role in controlling the rhythmic activity in sinoatrial node cells (5–8). Neuronal current is generally designated as hyperpolarization-activated current or I_h and contributes to controlling neuronal excitability. HCN channels contain a cyclic nucleotide–binding domain (CNBD) in the carboxyl terminus connected to the pore-forming S6 transmembrane segment via the C-linker (9). cAMP or cGMP binding to the CNBD induces a rightward shift of the voltage dependence of HCN4 channel activation (10, 11), thus increasing the current. Furthermore, all HCN channel isoforms contain a so-called HCN domain (HCND) at the N terminus. In HCN1 and HCN2, the HCND has been suggested to physically interact with both CNBD and voltage-sensor domain (VSD) to stabilize the closed pore in the setting of a depolarized voltage sensor (9, 12). Although there is no direct evidence demonstrating that this interaction is also occurring in HCN4 channels, the high similarity among the sequences of HCN1, HCN2, and HCN4 channels in these regions suggests that the HCND also exerts the same function in HCN4 channels. HCN family members differ in their sensitivity to cAMP, opening kinetics, and preferential tissue distribution (5). It is generally accepted that in all

The authors declare no competing interest.

This article is a PNAS Direct Submission.

[1]A.C.-C. and F.P. contributed equally to this work.

[2]R.C. and E.D. contributed equally to this work.

[3]To whom correspondence may be addressed. Email: rcaballero@ucm.es.

This article contains supporting information online at https://www.pnas.org/lookup/suppl/doi:10.1073/pnas.2305135120/-/DCSupplemental.

Published November 30, 2023.

mammalian species studied so far, HCN4 was found to be the main HCN channel isoform in the sinoatrial node, although HCN1 and HCN2 isoforms are also present (2, 13, 14). However, there are data suggesting that HCN1 is the predominant isoform expressed in the human sinoatrial node (15, 16).

In a large Spanish family with IST, we identified a mutation (p.V240M) within the HCND of HCN4 channels. Understanding the pathophysiology of IST is crucial to find a treatment for this debilitating condition. For its part, the role in cardiac pacemaking and the gating properties of HCN4 channels are currently not fully understood. Thus, we decided to clinically study all family members and functionally analyze the p.V240M HCN4 mutation through biochemical and electrophysiological approaches even at the single-channel level. Our results demonstrated that p.V240M is a naturally occurring HCND mutation causing an increased inward current flow during diastole accounting for the faster-than-normal heart rate of all carriers, that was reversed with treatment with ivabradine, a selective HCN channel blocker (13). Therefore, p.V240M is the second HCN4 gain-of-function mutation described in the literature (17), although it increases the I_f by a mechanism completely different from that of p.R524Q. Moreover, at the molecular level, our findings demonstrate the critical importance of the HCND in the gating of HCN4 channels. The results here presented strengthen the importance of genetic and functional studies in families carrying mutations with uncertain significance since they allow to the implementation of a personalized treatment and help in understanding the mechanisms controlling human cardiac electrophysiological properties.

Results

Clinical and Genetic Characteristics of the Patients. The proband (III.2 in Fig. 1*A*) is a 35-y-old female with a mean 24-h HR of 106[17] (mean[SD]) bpm (Table 1 and Fig. 1*B*). After a thorough evaluation, no reversible causes of sinus tachycardia were found (i.e., hyperthyroidism, anemia, diabetes, orthostatic hypotension, infections, and drug abuse), thus establishing the diagnosis of IST. The echocardiogram and cardiac magnetic resonance (CMR) showed mild systolic dysfunction [left ventricular ejection fraction (LVEF) = 43%] and no gadolinium enhancement. No signs of left ventricular noncompaction or hypertrabeculation were found. Her resting HR and electrocardiographic (ECG, in at least three different recordings) and cardiac structural parameters are described in *SI Appendix*, Table S1. Clinical evaluation of her relatives revealed that her father (II.1), two siblings (III.1 and III.4), two sons (IV.4 and IV.5), and three nieces (IV.1, IV.8, and IV.9) also fulfilled diagnostic criteria of IST (Table 1 and Fig. 1). Six more relatives were also clinically studied and none of them was diagnosed with IST (Table 1). No significant electrocardiographic or structural findings were detected in any of the IST patients (*SI Appendix*, Table S1). However, all adults with IST (five out of nine) had reduced LVEF without gadolinium enhancement, whereas children did not have cardiac dysfunction (Table 1 and Fig. 1). As expected, the HR of children was higher than that of adults (mean 24-h HR: 115.2[5.3] vs. 102.7[2.1] bpm, $P < 0.05$, $n \geq 4$). Patients IV.4 and IV.8 were diagnosed with fetal tachycardia with HR at 160 to 170 bpm at birth (>98 percentile). The proband's aunt (II.2) had died after heart transplant due to a congenital heart defect.

These data suggested that, in this family, there was a genetic component responsible for the IST. Next-generation sequencing (*SI Appendix*, Table S2) of the proband identified the pathogenic (according to the guidelines for the interpretation of variants, *SI Appendix*, Table S3 and *Methods*) heterozygous 15,73659894,C,T

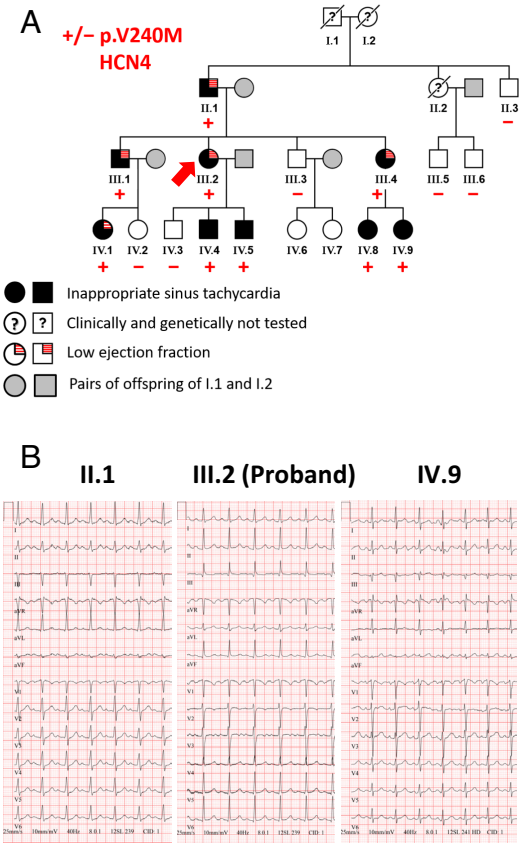

Fig. 1. A family with inappropriate sinus tachycardia (IST). (*A*) Pedigree of the IST proband's family. The arrow indicates the proband (III.2); circles and squares represent females and males, respectively. (*B*) Twelve-lead ECGs of II.1, III.2, and IV.9 family members (paper speed: 25 mm/s).

(NM_005477.3:c.718G>A) variant in *HCN4* gene encoding p.V240M HCN4. The mutated residue is highly conserved among different species and lies in the HCND of the protein (*SI Appendix*, Fig. S1). The p.V240M variant has been previously annotated with an allele frequency of 0.000003982 (https://gnomad.broadinstitute.org, accession date: 06/27/2023) since it was detected on a single allele in a South Asian subject. Cascade screening demonstrated the genotype–phenotype co-segregation of the *HCN4* variant (Fig. 1*A*). All carriers except II.1, who refused any treatment, were initially treated with ivabradine alone (7.5 mg twice daily for adults and 5 mg twice daily for the youngest carrier) with a significant response in terms of mean 24-h HR decrease (94[7] vs. 109[7.9], $P < 0.05$) and improvement in symptoms and quality of life (Table 1). Three adult patients had their ivabradine dose reduced (5 mg twice daily) since they experienced mild weakness and dizziness, which are frequently associated to the use of this drug. Bisoprolol (5 mg twice daily), an antagonist of β-adrenergic receptors (beta blocker), was added to them to achieve a better HR control (from 91[1.5] before to 84[5] after bisoprolol).

Macroscopic Current Analysis. To test whether the p.V240M HCN4 mutation underlies the IST in this family, we functionally analyzed this variant. Fig. 2*A* shows macroscopic HCN4 current (I_{HCN4}) traces generated in three different Chinese hamster ovary (CHO) cells transfected with WT, p.V240M, and the combination of WT and p.V240M HCN4 channels (0.5:0.5 ratio). I_{HCN4} generated by p.V240M channels (measured at the end of 4-s pulses) was significantly greater than that generated by WT channels in a wide range of membrane potentials including those between −90 and −60 mV (−3.1 ± 1.4 vs. −7.7 ± 2.7 pA/pF at −60 mV; $P < 0.05$, n = 5)

Table 1. Clinical characteristics of the family members studied

Patient	Gender	Age at diagnosis (years)	Symptoms	Heart rate (bpm)		Functional class (NYHA)		LVEF (%)		Treatment	
				Baseline	A. T.						
				Mean 24 h	**Mean 24 h**	Baseline	A. T.	Baseline	A. T.	Ivabradine (mg BID)	Bisoprolol (5 mg BID)
Carriers											
II-1	M	65	Yes	95[13]		III	III	23			
III-1	M	39	No	100[15]	90[4]*	I	I	45	55	5	+
III-2 (#)	F	35	Yes	106[17]	78[5]*	III	I	43	55	5	+
III-4	F	28	Yes	101[13]	85[8]*	I-II	I	45	56	5	+
IV-1	F	21	No	103[10]	82[19]*	I	I	51	57	7.5	
IV-4	M	11	Yes	111[12]	94[12]*	I	I	60	60	7.5	
IV-5	M	6	No	122[15]	101[10]*	I	I	64	64	5	
IV-8	F	12	No	112[14]	103[14]*	I	I	60	59	7.5	
IV-9	F	10	Yes	117[12]	102[12]*	I	I	63	64	7.5	
Noncarriers											
II-3	M	57		80[15]				55			
III-3	M	42		79[13]				56			
III-5	M	43		46[14]				56			
III-6	M	41		79[11]				55			
IV-2	F	11		84[15]				59			
IV-3	M	17		75[15]				58			

#: Proband; A.T.: 3 mo after initiation of treatment; BID: twice daily; bpm: beats per minute; F: female; HR: heart rate; LVEF: left ventricular ejection fraction; M: male; NYHA: New York Heart Association. Mean 24 h HR data are presented as mean[SD]. Student's *t* test followed by Pearson correlation tests. *$P < 0.05$ vs. baseline.

(Fig. 2 *A* and *B* and Table 2). Interestingly, densities of I_{HCN4} generated by the cotransfection of WT and p.V240M channels were also significantly greater than those of WT channels (Fig. 2 *A* and *B* and Table 2). Fig. 2*C* demonstrates that the p.V240M variant did not modify the selectivity of HCN4 channels since the reversal potential (E_{rev}) of the current (calculated from the intersection of the linear regression of the relationship of fully activated channels with the abscissa) was not altered ($P > 0.05$, $n \geq 5$) (Table 2).

Fig. 2 *D* and *E* depict the I_{HCN4} activation (τ_{act}) and deactivation (τ_{deact}) time constants, respectively (obtained as described in *SI Appendix, Methods*), as a function of the membrane potential. It can be observed that, at different membrane potentials, currents generated p.V240M and WT+p.V240M HCN4 channels activated faster and deactivated slower than those generated by WT channels ($P < 0.05$, $n \geq 5$) (Table 2).

Voltage Dependence of the Activation of p.V240M HCN4 Channels. Fig. 3*A* shows typical I_{HCN4} generated by WT+p.V240M channels when applying the protocol shown at the top, which consists of a hyperpolarizing test pulse of variable duration (from 1.5 s at −160 mV to 12 s at −20 mV) followed by a 1.5 s pulse to 0 mV from a holding potential of −40 mV. Fig. 3*C* shows superimposed tail currents elicited by the 1.5-s pulse to 0 mV generated by WT and p.V240M channels. Non-steady-state activation curves of WT, p.V240M, and WT+p.V240M channels were constructed by plotting the normalized tail amplitudes as a function of the membrane potential of the test pulse. Fig. 3*B* demonstrates that the p.V240M variant either alone or in combination with WT channels, significantly and markedly shifted the midpoint (Vh) of the activation curve to more depolarized membrane potentials as assessed by Boltzmann fits (Table 2).

Interestingly, effects produced by the p.V240M variant are quite similar to those produced by cAMP (10) and thus, we hypothesized that the mutation increases I_{HCN4} by augmenting HCN4 channel affinity for cAMP. Since HCN4 activation is not affected by cAMP when channels are expressed in CHO cells (18), we tested our hypothesis in human embryonic kidney-293 (HEK293) cells that were exposed to a saturating cAMP concentration (10 μM) in the whole-cell pipette solution. As expected, cAMP significantly shifted the activation curve of WT HCN4 channels toward depolarizing potentials (Fig. 3*D*). In HEK293 cells the Vh of p.V240M HCN4 channel activation (−86.9 ± 1.9 mV) was also significantly more depolarized than that of WT channels (−107.0 ± 4.2 mV, $n \geq 5$, $P < 0.05$). Importantly, voltage-dependent activation of p.V240M channels was significantly right shifted in the presence of cAMP (−68.7 ± 0.8 mV, $n \geq 4$, $P < 0.05$) (Fig. 3*E*). Furthermore, Vh values in the absence and presence of cAMP of I_{HCN4} generated by WT+p.V240M subunits (−96.8 ± 2.7 and −78.7 ± 1.4 mV, respectively) lay in between those of WT and p.V240M channels ($n \geq 7$, $P < 0.05$) (Fig. 3*F*).

Effects of the p.V240M HCN4 Mutation on the Membrane Expression. To analyze whether an increase of the expression of p.V240M HCN4 channels at the plasma membrane accounted for the I_{HCN4} increase, we conducted a cell surface biotinylation assay (Fig. 4) measuring the levels of expression of total HCN4 protein (inputs) and membrane fraction (biotinylated) by Western blot (Fig. 4*A*). Fig. 4*B* shows the densitometry of the relative surface expression of WT and p.V240M HCN4 subunits and demonstrates that there were no significant differences in the expression of mutated and WT channels ($P > 0.05$, $n = 5$).

Single-Channel Properties of p.V240M HCN4 Channels. Fig. 5 shows representative single-channel traces recorded in CHO cells at −90 mV in the absence (control, *Top* panels) or the presence (*Bottom* panels) of ivabradine (5 μM), a selective I_f inhibitor (13), using the cell-attached configuration. In all experiments, we confirmed that ivabradine perfusion completely inhibited the unitary HCN4 current (i_{HCN4}). Importantly, the p.V240M

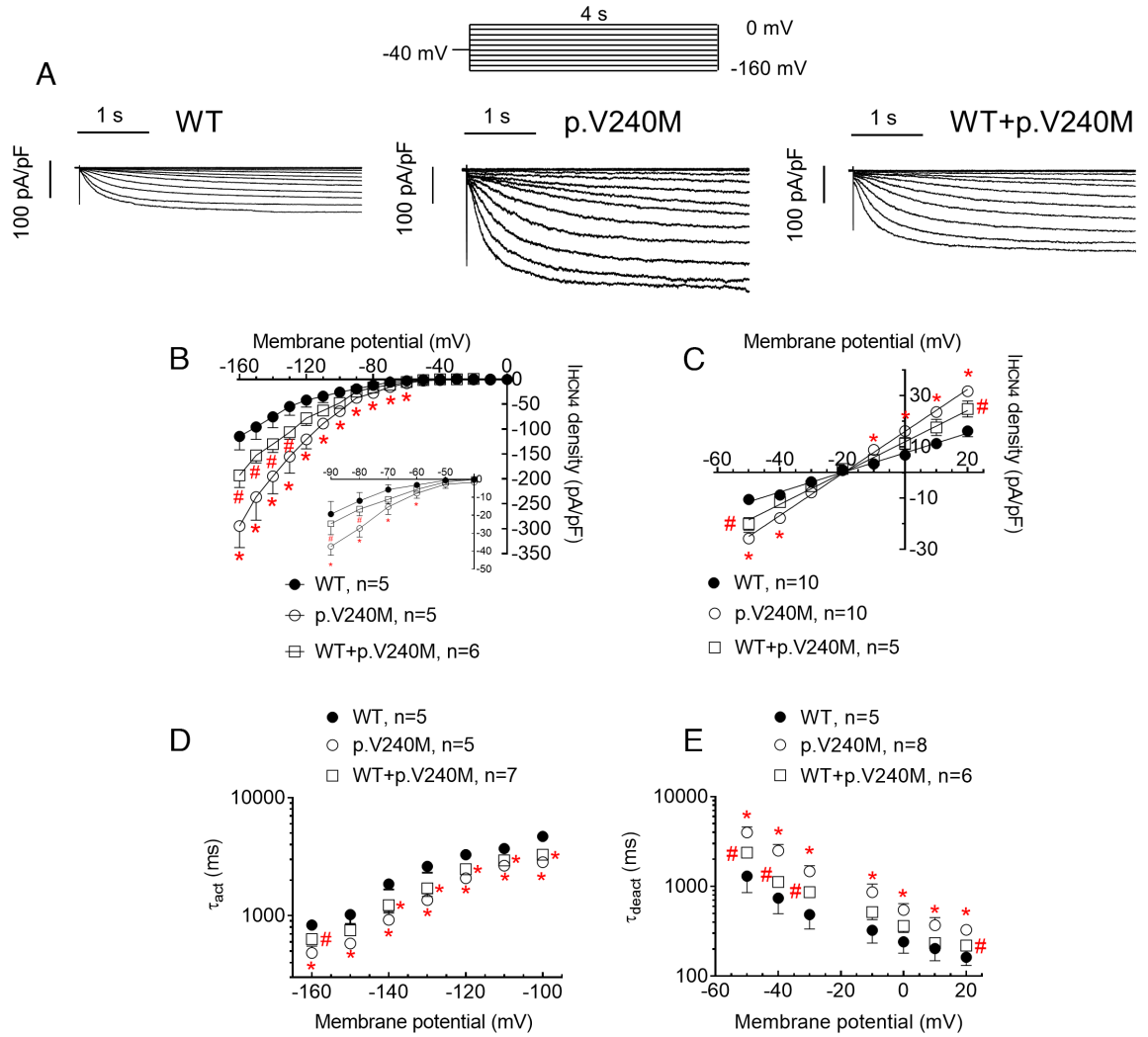

Fig. 2. Macroscopic currents generated by WT, p.V240M, and WT+p.V240M HCN4 channels. (*A* and *B*) I_{HCN4} traces (*A*) and density–voltage relationships (*B*) generated in CHO cells transiently expressing WT, p.V240M, and WT+p.V240M HCN4 channels by applying the protocol depicted at the top. The *Inset* in *B* shows data at potentials between −90 and −50 mV in an expanded scale. (*C*) Fully activated I_{HCN4} density–voltage relationships generated by WT, p.V240M, and WT+p.V240M channels. Continuous lines represent a linear regression fit to the data. (*D* and *E*) Time constants of I_{HCN4} activation (*D*) and deactivation (*E*) measured at different membrane potentials. In (*B–E*), each point represents the mean ± SEM of ≥5 experiments/cells from ≥3 dishes. **P* < 0.01 vs. HCN4 WT. #*P* < 0.05 vs. HCN4 WT and *P* < 0.05 vs. p.V240M. ANOVA followed by Tukey's test and multilevel mixed-effects model.

mutation did not modify the HCN4 channel sensitivity to ivabradine (*SI Appendix*, Fig. S2). No single-channel recordings were obtained in non-transfected cells since they do not express endogenous HCN4 channels (Fig. 5 *A* and *D*). i_{HCN4} generated by WT channels (Fig. 5*B*) was characterized by spontaneous openings followed by periods of channel closure yielding mean f_o

Table 2. Effects of p.V240M variant on the time- and voltage-dependent properties of macroscopic and unitary HCN4 currents recorded in CHO cells

Whole-cell							
HCN4	E_{rev} (mV)	τ_{act} at −160 mV (ms)	V_{hact} (mV)	k_{act}	I_{HCN4} density −160 mV (pA/pF)	I_{HCN4} density −60 mV (pA/pF)	
WT	−20.2 ± 0.8	832 ± 43	−115.4 ± 5.6	10.6 ± 0.6	−116.4 ± 35.0	−3.1 ± 1.4	
p.V240M	−22.1 ± 2.4	483 ± 61*	−87.9 ± 1.9*	11.4 ± 4.5	−294.5 ± 43.2*	−7.7 ± 2.7*	
WT+p.V240M	−19.2 ± 1.4	634 ± 51#	−98.7 ± 1.5#	12.4 ± 1.7	−193.1 ± 24.8#	−5.5 ± 0.9	
Single-channel							
HCN4	τ_{OPEN} (ms)* (−90 mV)	τ_{CLOSED} (ms)* (−90 mV)	MOT (ms)	f_o (Hz)	P_o	i_{HCN4} −90 mV (pA)	γ (pS)
WT	17.8	68.1	36.2 ± 9.8	5.2 ± 1.1	0.11 ± 0.02	−1.6 ± 0.3	16.3 ± 2.7
p.V240M	9.3*	18.6*	17.1 ± 3.5*	13.2 ± 1.0*	0.23 ± 0.03*	−2.9 ± 0.4*	39.8 ± 4.2*

*These values are obtained by the fit of a monoexponential fit to the curves constructed with the respective mean values.
E_{rev}: reversal potential; f_o: open frequency; γ: single channel conductance; k_{act}: slope of the activation curve; MOT: mean open time; P_o: open probability; τ_{act}: time constant of I_{HCN4} activation; τ_{OPEN}: open time constant yielded by the fit of a monoexponential function to the open time histogram; τ_{CLOSED}: closed time constant yielded by the fit of a monoexponential function to the closed time histogram; V_{hact}: midpoint of the activation curve. Each value represents mean ± SEM of >5 cells/experiments from at least three different dishes in each group. Statistical comparisons were made by using ANOVA followed by Tukey's test (whole-cell) or using the *t* test (single-channel). **P* < 0.05 vs. WT; #*P* < 0.05 vs. p.V240M.

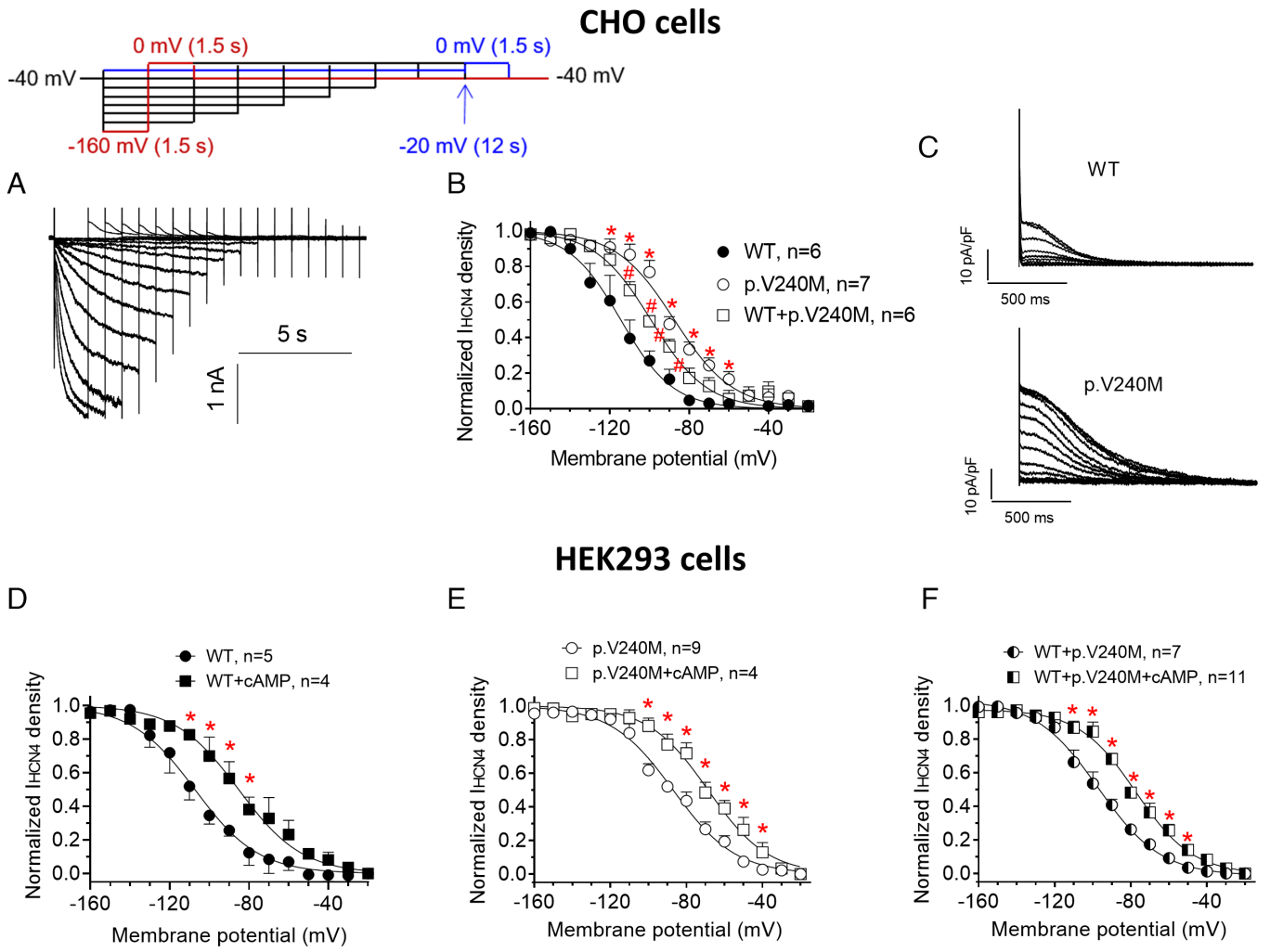

Fig. 3. Effects of p.V240M on the voltage dependence of I_{HCN4} activation. (*A*) Typical I_{HCN4} generated by WT+p.V240M channels when applying the protocol shown at the top, which consists of a test hyperpolarizing pulse of variable duration (from 1.5 s at −160 mV to 12 s at −20 mV) followed by a 1.5-s pulse to 0 mV from a holding potential of −40 mV. The first (−160 mV) and last (−20 mV) pulses of the protocol are shown in red and blue, respectively. (*B*) Non-steady-state activation curves of WT, p.V240M, and WT+p.V240M channels expressed in CHO cells constructed by plotting the normalized tail amplitudes as a function of the membrane potential of the test pulse. *$P < 0.05$ vs. HCN4 WT. #$P < 0.05$ vs. HCN4 WT and p.V240M. (*C*) Example of superimposed tail currents elicited by the 1.5-s pulse to 0 mV generated by WT and p.V240M channels. (*D*–*F*) Non-steady-state activation curves of WT (*D*), p.V240M (*E*), and WT+p.V240M (*F*) channels expressed in HEK293 cells in the presence or absence of 10 μM cAMP. *$P < 0.05$ vs. cells nondialyzed with cAMP. In (*B*) and (*D*–*F*), tail current densities were normalized and plotted against the membrane potential of the test pulse. Continuous lines represent the Boltzmann fit to the data. ANOVA followed by Tukey's test and multilevel mixed-effects model.

and P_o values of 5.2 ± 1.1 Hz and 0.11 ± 0.02 (n = 5), respectively (Fig. 6 *A* and *B* and Table 2). Conversely, i_{HCN4} generated by p.V240M channels was characterized by openings in bursts (Fig. 5*C*). Accordingly, both f_o and P_o significantly increased, while the mean open time significantly decreased compared to those of WT channels ($P < 0.05$, n ≥ 5) (Fig. 6 *A*–*C* and Table 2). Moreover, i_{HCN4} amplitude generated by p.V240M channels at −90 mV (Fig. 6*D*) and at all membrane potentials tested was significantly greater than that of WT channels (Fig. 6*E*, $P < 0.05$, n = 5). Fig. 6*E* shows that single-channel conductance (γ) derived from the linear regression of the current-voltage relationships of p.V240M channels was double than that of WT channels (Table 2). Importantly, γ here obtained for WT channels (16.3 ± 2.7 pS) is in agreement with that previously reported for HCN4 channels (19, 20).

To describe kinetic features of HCN channels, an allosteric model with five open and five closed states has been proposed (21). However, to compare the main features of the gating kinetics of WT and p.V240M channels at −90 mV, both close and open dwell-time histograms were fitted by monoexponential functions (*SI Appendix*, *Methods* and Fig. S3) in order to obtain the dominant time constant of the process. Table 2 and *SI Appendix*, Fig. S3 show that the mutation significantly reduced both the τ_{CLOSED} and the τ_{OPEN} ($P < 0.05$).

Mathematical Model of Human Sinoatrial Action Potentials. Fig. 7*A* shows human sinoatrial action potentials (APs) obtained when running the Fabbri–Fantini–Wilders–Severi (22) mathematical model (37 °C) considering the I_f generated by WT HCN4 channels. AP characteristics are described in *SI Appendix*, Table S4. I_f conductance was increased by 100 and 61.7% and the voltage-dependence of activation was shifted by +27.5 and +16.7 mV to simulate the effects of p.V240M and WT+p.V240M HCN4 channels, respectively (*SI Appendix*, *Methods*). Spontaneous firing frequency of the AP averaged 73.8 bpm and it was doubled (179.6 bpm) when APs were modeled considering the I_f generated by p.V240M channels (Fig. 7*A*). The acceleration of the pacemaker frequency is a consequence of the huge increase in the I_f density produced by the mutation (Fig. 7*B*). Interestingly, I_f currents generated when considering the heterozygous presence of p.V240M

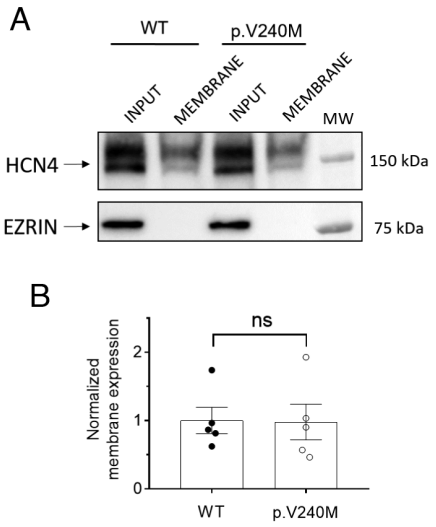

Fig. 4. Membrane expression of WT and p.V240M HCN4 channels. Representative western blot images (*A*) and densitometric analyses (*B*) of biotinylation assays showing the total (input) or surface (membrane) expression of HCN4 in CHO cells expressing WT or p.V240M channels. The cytosolic protein ezrin was used as a negative control. In (*B*), each dot represents one experiment and each bar the mean ± SEM of five experiments.

channels are also greater than those generated by WT channels (Fig. 7*B*), the firing frequency reaching 128.5 bpm (Fig. 7*A*).

Molecular Modeling. To test the possible molecular mechanism responsible for the gain-of-function effects of p.V240M, we have mutated in silico a human HCN4 crystalized structure (PDB: 6GYN, Fig. 8 and *SI Appendix*). In HCN4 channels, the HCND is anchored to the VSD by means of F229, whose aromatic side chain is inserted between transmembrane helices S1 and S4 in a hydrophobic pocket formed by I404 and M407 in S4, and Y258 in S1 (Fig. 8 *B* and *C* and *SI Appendix*). Our molecular modeling demonstrates that the mutation introduces a slight torsion of the aromatic group of F229 and prevents the H-bond between K228 in HCND and Y409 in S4 (Fig. 8*C*). These effects might weaken the interaction between HCND and VSD. Moreover, the results demonstrated that the interaction between CNBD and HCND is not affected by the p.V240M mutation (Fig. 8*C* and *SI Appendix*).

Discussion

In this study, we identified several members of a family diagnosed with IST carrying a gain-of-function *HCN4* variant. The results of our functional analysis demonstrated that p.V240M variant markedly increases the f_o and the P_o and depolarizes the voltage dependence of HCN4 channels' activation. Thus, the mutation increases I_{HCN4} by altering the gating without modifying the channel sensitivity for cAMP and ivabradine or the membrane expression. All these effects account for the huge increase of I_{HCN4}, which, in turn, explains the IST of the affected family members, who were treated with ivabradine, which reversed IST and tachycardia-induced cardiomyopathy.

As described above, the p.V240M mutation is, to the best of our knowledge, the second HCN4 gain-of-function mutation described in the literature. The first one was the p.R524Q HCN4 variant, that increases the channel affinity for cAMP and was described in an Italian family with symptomatic sinus tachyarrhythmia (17). Conversely, many loss-of-function heterozygous mutations in the *HCN4* gene have been associated with sinus bradycardia that can be accompanied, or not, with atrial fibrillation, atrioventricular block, structural diseases such as noncompaction cardiomyopathy, and even QT prolongation (7, 23–32). As mentioned, there has been important controversy regarding the role of HCN4 isoforms in generating human I_f and in pacemaking of the sinoatrial node. There are reports demonstrating that the predominant HCN isoform at both the protein and RNA levels is HCN1 (15, 16). However, only a few data on the literature suggested the contribution of HCN1 variants to HR. One of them is a case report (33) showing two rare *HCN1* heterozygous variants identified in a young patient with profound sinus bradycardia. A second report identifies a polymorphic *HCN1* variant that was associated with HR variability and schizophrenia (34). Conversely, dysfunctional HCN1 channels seem to play an important role outside of the heart in different forms of epilepsy and neuropathic pain (35, 36). Our results add further support to the contention that, in humans, HCN4 channels critically determine I_f density in sinoatrial cells, thus regulating HR.

The V240 residue is located in the N terminus, and variants in this domain are less commonly described than in the pore and C-terminal regions of HCN4 channels. The HCND is formed by a stretch of 45 aminoacids directly preceding the S1 transmembrane

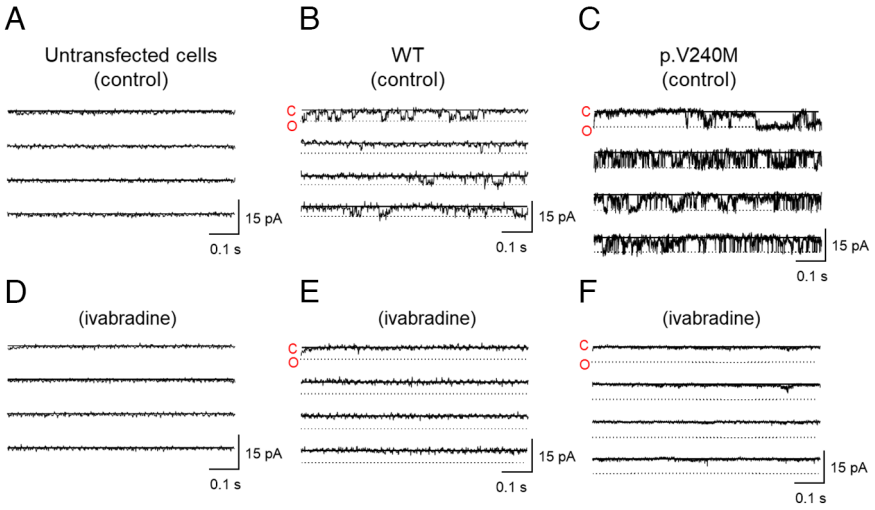

Fig. 5. Single-channel recordings generated by WT and p.V240M HCN4 channels. Single-channel recordings obtained by applying 3-s pulses from −35 to −90 mV in cells expressing or not (*A*) WT (*B*) or p.V240M (*C*) HCN4 channels in the absence and presence (*D–F*) of ivabradine 5 μM. Continuous and dotted lines represent the current amplitude generated by closed (C) and open (O) channels, respectively.

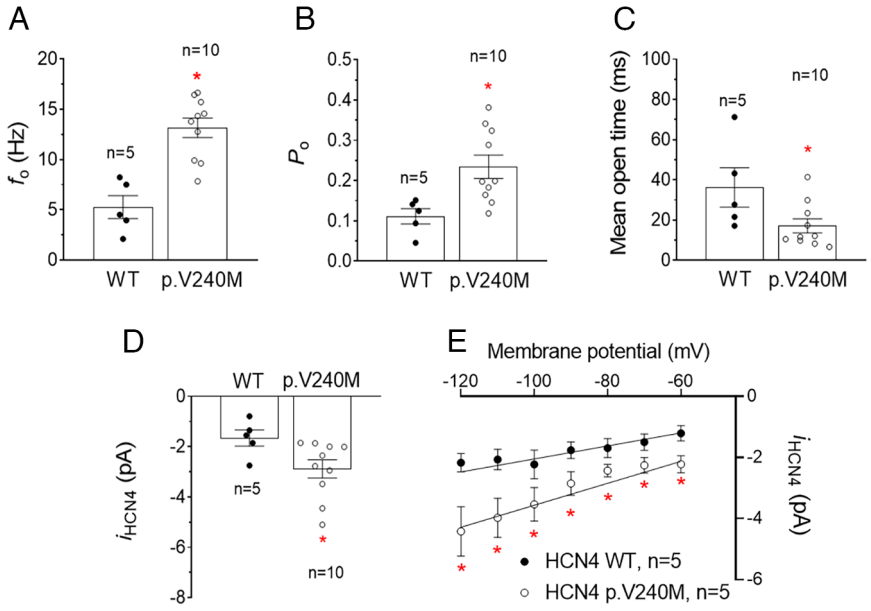

Fig. 6. Gating properties of WT and p.V240M HCN4 channels. Mean f_o (*A*), P_o (*B*), and open time (*C*) for i_{HCN4} recorded in cells expressing WT or p.V240M HCN4 channels by applying 3-s pulses from −35 to −90 mV. (*D*) i_{HCN4} amplitude generated by WT and p.V240M channels after applying pulses to −90 mV. (*E*) i_{HCN4}-voltage relationships generated by WT and p.V240M channels. In (*A*–*D*), each dot represents one experiment/cell and each bar the mean ± SEM of n experiments/cells as indicated in the figure. In (*E*), each point represents the mean ± SEM of 5 experiments/cells. *$P < 0.05$ vs. WT. Student's *t* test and multilevel mixed-effects model.

segment that consists of three α-helices (HCNa, HCNb, and HCNc) (*SI Appendix*, Fig. S1) (9). The V240 residue is actually located in the HCNc α-helix. The HCND could act as a sliding crank that converts the planar rotational movement of the CNBD into a rotational upward displacement of the VSD mechanically coupling thus, the CNBD and the VSD (12, 37). HCND normally keeps the VSD in a position, which is unfavorable for channel opening (12). Thus, these results suggest that p.V240M mutation limits the inhibitory action of the HCND on the VSD and would explain the marked positive displacement (≈20 mV) of the activation curve of p.V240M channels.

The cAMP-induced movement of the C-linker produced by the binding of cAMP to the CNBD is transmitted via the HCND to the VSD, lowering the energy barrier for channel opening (12, 37). The mutants that disrupt the contact between the CNBD and the HCND eliminate the effect of cAMP on channel activation (12, 37). The p.V240M mutation does not seem to affect the interaction between CNBD and HCND. The latter would explain why p.V240M channels are sensitive to cAMP. Interestingly, our results demonstrated that p.V240M mutation markedly increases single HCN4 channel conductance, an effect that is beyond the positive shift of the activation curve. We propose that the mutation introduces changes in the pore region that controls the conductance of the channel, even when the channel selectivity is not affected. In summary, our results contribute to the understanding of the role of HCND in the distinctive biophysical properties of these channels.

The HCND is also necessary for the folding and trafficking of the channel to the plasma membrane (12, 37). To the best of our knowledge, the only naturally occurring HCND mutation described

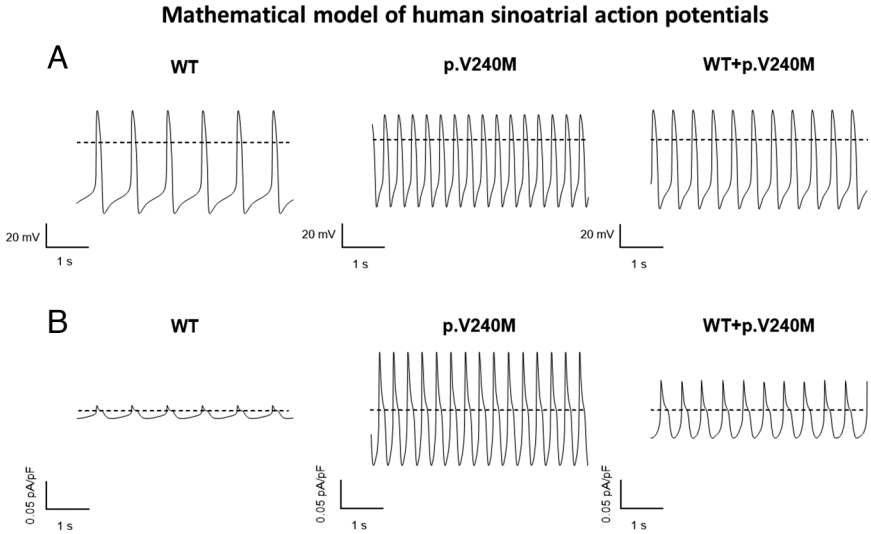

Fig. 7. Mathematical model of human sinoatrial node cell action potential. (*A* and *B*) APs (*A*) and I_f (*B*) obtained when running the model under basal conditions (WT; *Left*), or after introducing the experimentally measured I_{HCN4} changes induced by p.V240M alone (center) or together with WT (*Right*). The dotted lines represent the zero membrane potential (*A*) and current (*B*) levels.

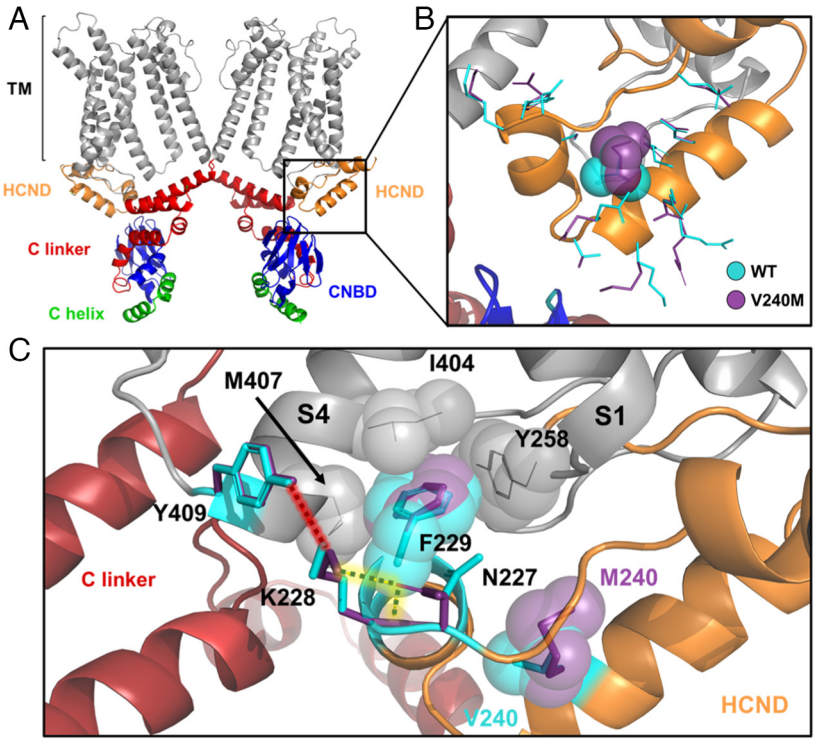

Fig. 8. Molecular modeling of WT and p.V240M HCN4 channels. (*A*) Ribbon representation of the cryo-EM structure of human HCN4 (PDB: 6GYN). Only two diagonal subunits are shown for clarity. The transmembrane segments (TM) are gray, the HCND is orange, the C-linker is red, the CNBD is blue, and the distal C helix is green. (*B*) Close view of superimposed WT and V240M models (color coded as in *A*). Sticks representation shows amino acids side-chains from WT (cyan) and V240M (purple). V240 and M240 are shown as spheres. (*C*) Interaction of HCND with the VSD showing the hydrophobic interactions of F229 with I404 and M407 from TM S4 (VSD) and Y258 from the loop connecting HCND to TM S1, and polar contacts of K228 and Y409 in WT (red dashed line) or K228 and N227 in V240M (yellow dashed line). Spheres represent the van der Waals surface occupied by the side chains.

so far in HCN4 channels is p.P257S, which was identified in patients with early-onset atrial fibrillation (26). p.P257S channels present a trafficking defect, being retained at the endoplasmic reticulum (26). Conversely, the p.V240M mutant is properly expressed in the membrane suggesting that p.V240M mutation does not affect the folding and trafficking of HCN4 subunits.

To the best of our knowledge, disease-causing mutation affecting the residues equivalent to V240 in HCN1 (V120), HCN2 (V189), and HCN3 (V71) channels are scarce if any (*SI Appendix*, Table S5). However, different naturally occurring mutations have been annotated, up to date, in the ClinVar repository (https://www.ncbi.nlm.nih.gov/clinvar/) that lay in the HCND of HCN1-4 channels (*SI Appendix*, Table S5). Many of these variants were found in patients with neurological (familial febrile seizures, neurodevelopmental delay, or infantile epileptic encephalopathy for *HCN1* and *HCN2* variants) or cardiac (Brugada syndrome for *HCN4* variants) inherited diseases. However, as far as we know, none of them were functionally studied. Thus, there are no data indicating whether these variants are gain- or loss-of-function variants, and it is difficult to establish a genotype–phenotype relationship. However, the findings suggest that maintaining the integrity of this region is critical for channel function both in the central nervous system or in the heart.

Clinical Implications

IST is barely associated with heart dysfunction and tachycardia-induced cardiomyopathy (1, 38), although some cases have been already reported (39, 40). Furthermore, *HCN4* mutations have been associated with noncompaction cardiomyopathy (28, 30–32), but no signs of hypertrabeculation were found with CMR imaging or echocardiography in this family. Affected adults in our family had systolic ventricular dysfunction that reversed with the treatment. Thus, we assumed that the high HR and the duration of the arrhythmia (present from childhood but being documented even before birth in two patients) could have been the major contributors to cardiac dysfunction in our patients. Regarding treatment of IST, carriers were treated with ivabradine, since previous reports demonstrated that it reduced HR and improved quality of life in patients with IST (41). Interestingly, the HR reduction in our study with ivabradine alone was ≈14%, which is similar to that obtained previously in patients with IST of an unknown origin (41, 42). Responsiveness of our patients to ivabradine can be explained considering that sensitivity of p.V240M channels was identical to that of WT HCN4 and is an example of the importance of genetic and functional information for the design of personalized therapies in patients with inherited arrhythmogenic syndromes.

The degree of activation of I_f at the end of an AP determines the steepness of phase 4 depolarization and, hence, the frequency of AP firing (28). Thus, it seems reasonable to assume that the gain-of-function p.V240M mutation is responsible for an increase in sinoatrial node automaticity and the IST of the affected subjects in this family. The penetrance and expressivity of the mutation in this family is complete, which is quite infrequent among patients who carry a pathogenic mutation related to primary arrhythmogenic syndromes.

Limitations

Macroscopic and microscopic currents were recorded at room temperature, and under this condition, the I_{HCN4} activation kinetics is slower, and the V_h of the activation curves are more negative than those obtained at 37 °C (18, 32). The slow kinetics preclude reaching the steady-state activation of the current even at very negative

potentials but we could not increase the duration of the steps without instability and cell death. Therefore, differences in the voltage dependence of WT and p.V240M channels activation could partially result from the combination of changes produced by the mutation in both voltage dependence and rate of I_{HCN4} activation. Furthermore, for simulating the WT+p.V240M I_f and sinoatrial APs, we ran the model by introducing data obtained at room temperature, while the control I_f values of the Fabbri–Fantini–Wilders–Severi are those of the current recorded at 37 °C. Furthermore, we fitted both closed and open dwell-time histograms by monoexponential functions. This allowed us to compare the dominant time constant of the gating kinetics of WT and p.V240M channels. However, this simplification could not represent the kinetic process of HCN channels which has been modeled by a multistate scheme comprising five open and five closed states (21).

Conclusions

Our results support the view that individuals carrying the p.V240M mutation present higher than normal I_{HCN4}. This variant increases I_{HCN4} by an unique mechanism that implies the alteration of the gating without modifying the channel sensitivity for cAMP or the membrane expression. Therefore, p.V240M is a naturally occurring gain-of-function HCND variant, which explains the faster-than-normal HR and IST of the carriers. The clinical, genetic, and functional study of the variant led to the establishment of the personalized treatment with ivabradine for all carriers and contribute to shed light on the understanding of the pathophysiology of IST.

Materials and Methods

Study Approval. Clinical evaluation of the proband and her relatives was approved by the Investigation Committee (ref: CEIM/CEI/3-19 [12/4/19]) of the Hospital Universitario Virgen de las Nieves (Granada, Spain) and conforms to the principles outlined in the Declaration of Helsinki. Each participant gave written informed consent for clinical and genetic evaluation.

Clinical Study. The proband and relatives of a Spanish family with several members diagnosed with IST and left ventricular systolic dysfunction were evaluated at the "Hereditary cardiovascular disease unit" in the Cardiology Department of the Hospital Universitario Virgen de las Nieves. Trained personnel performed at least three ECG at rest to the proband and to all the family members who gave their written informed consent (*SI Appendix*, Table S1). Family members either diagnosed or not with IST underwent a serial 24-h ECG monitoring (at least two for patients diagnosed with IST). CMR was performed only to adult family members with IST. Three months after initiation of medical therapy with ivabradine (7.5 mg twice daily in adults, 5 mg twice daily in children) or ivabradine (5 mg twice daily) plus bisoprolol (5 mg twice daily), the 24-h Holter monitoring and echocardiogram were repeated for every patient, and the findings were compared with those obtained before treatment. The size of the chamber, quantifications, and severity partition cut-offs of left ventricular dysfunction were measured according to the current guidelines. IST was defined as fast sinus rates (>100 bpm at rest or >90 bpm on average over 24 h) not due to underlying causes (38). Thus, prior to IST diagnosis, other causes such as hyperthyroidism, anemia, diabetes mellitus, orthostatic hypotension, infections, and drug abuse were ruled out. A full pedigree was obtained collecting information such as cardiac events (sudden cardiac death, heart transplantation, or device implantation), cases of IST, or systolic dysfunction of unknown etiology and any kind of cardiomyopathy across four generations. Echocardiographic, ECG, and imaging recordings were interpreted by experienced cardiologists, blinded to the genetic and clinical data of the participants. QT values were corrected using the Bazett's formula.

Next-Generation and Sanger Sequencing. DNA was extracted from whole blood of the proband, and the genetic analysis was conducted by using a next-generation sequencing panel including 197 genes (*SI Appendix*, Table S2) following described procedures from our lab (43, 44). Pathogenicity of the found variants was established according to the current recommendations of the American College of Medical Genetics and Genomics and the Association for Molecular Pathology (45). Other exonic non-synonymous variants found are described in *SI Appendix*, Table S3. A phenotype–genotype segregation study was conducted through cascade screening among available relatives with Sanger genetic study (43).

Cell Culture and Transfection. CHO (30, 43) and HEK293 (46) cells were grown as previously described and transiently transfected with 0.5 (single-channel recordings) or 1.6 μg (macroscopic current recordings) of human WT or mutant *HCN4* (NM_005477.3) cDNA subcloned into the pIRES2 DsRed-Express2 (Takara-Bio) vector kindly provided by Michael Koenen (Max Planck Institute for Medical Research, Heidelberg, Germany) (30, 47). The p.V240M HCN4 mutation (NP_005468.1) was introduced by using the QuikChange Site-Directed Mutagenesis kit (Agilent) and confirmed by direct DNA sequencing (Secugen S.L.). In some experiments, WT and p.V240M HCN4 were cotransfected (WT+p.V240M) at a 0.5:0.5 ratio (0.8 μg each). To minimize the influence of the expression variability, each construct was tested in a large number of cells obtained from at least three different cell batches. Moreover, to avoid putative interferences of culture conditions (passage number, cell density, etc.), currents generated by cells expressing WT, p.V240M, and WT+p.V240M channels were always recorded in parallel.

Recording Techniques. ***Macroscopic current recordings.*** Macroscopic currents were recorded in CHO cells at room temperature (21 to 23 °C) by means of the whole-cell patch-clamp technique using Axopatch-200B patch clamp amplifiers and pCLAMP 10 software (Molecular Devices) (30, 43, 46). Micropipette resistance ranged 3 to 5 MΩ when filled with the internal solution and immersed in the external solution (see composition in *SI Appendix*, *Methods*). Under our experimental conditions, no significant voltage errors (<5 mV) due to series resistance were expected with the micropipettes used. Current amplitude measured in each experiment was normalized to membrane capacitance to obtain current densities. In a subset of experiments, the consequences of the p.V240M variant on the shift of the voltage-dependent activation produced by of 3′,5′-cyclic adenosine monophosphate (cAMP) were analyzed in HEK293 cells. The effects of different concentrations of ivabradine (0.1 to 3 μM) were determined in CHO cells transfected with WT, p.V240M or WT+p.V240M HCN4 channels.

Single-channel recordings. Single-channel currents were recorded in CHO cells at room temperature (21 to 23 °C) by means of the cell-attached patch-clamp configuration using Axopatch-200B patch clamp amplifiers and pCLAMP 10 software (19, 20, 46). Patch pipettes (resistance between 5 and 10 MΩ) were pulled from 1.5 mm o.d. borosilicate capillary tubes (Harvard Apparatus Ltd.). The apparent number of active channels in a patch was determined by visual inspection of the current traces and patches with more than one channel were discarded. The experimental conditions were optimized to reduce the number of active channels on each recording by increasing the tip resistance of the pipettes ≈threefold compared to whole-cell recordings. Under these conditions, only 10% of cells with active channels had more than one channel. At the end of each experiment, the HCN channel blocker ivabradine (5 μM) (48) was added to the external solution to specifically abolish single-channel currents generated by HCN4 channels.

Biotinylation Assay. A biotinylation assay was conducted in CHO cells using procedures previously described (49). At the point of 48 h after transfection of HCN4 WT or p.V240M, CHO cells were biotinylated using EZ Link Sulfo-NHS-SS-Biotin (ThermoFisher Scientific). After sample processing, the obtained extract was incubated with Streptavidin Sepharose (50 μL, GE Healthcare Life Sciences), and the biotinylated fraction was separated by centrifugation. Thereafter, HCN4 and ezrin proteins were detected by western blot following previously described procedures (43, 44, 49) using rabbit polyclonal anti-HCN4 (1:1,000; 55224-1-AP, Proteintech) and mouse monoclonal anti-ezrin (1:400; ab4069, Abcam) primary antibodies. Expression of the proteins in the biotinylated (membrane) fraction was normalized to the input expression.

Mathematical Modeling of Human Sinoatrial Node Action Potential. For simulating I_f and APs generated by human sinus node cells (37 °C), we employed the Fabbri–Fantini–Wilders–Severi model previously validated and used for similar purposes (22). The model was obtained from the CellML model repository and run using OpenCell software. The model was run keeping all parameters at their default values (WT) and after introducing the experimentally measured changes produced by p.V240M HCN4 or WT + p.V240M HCN4 on the macroscopic I_f. The increase in I_f conductance was incorporated in the g_f parameter of the model, while the depolarizing shift in the voltage dependence of activation was

implemented by introducing the shift value in the y_{shift} parameter. Since gating kinetics would undergo the same voltage shift, further changes in the activation or deactivation time constants were not incorporated.

Molecular Modeling. To estimate the conformational changes produced by the p.V240M HCN4 mutation, a molecular modeling using the crystallized structure of human HCN4 (PDB: 6GYN) was performed. Model refinement, in silico mutagenesis, and energy calculation were done with FoldX Suite (version 4.0, foldxsuite.crg.eu) and the RepairPDB protocol (50). Default parameters of the software were used except temperature, pH, ionic strength, and VdW design that were set to 298 K, 7.0, 5, and 0, respectively. When the model running was completed, the software provided different conformations with different energies and the conformation of the mutated form with the lowest energy was chosen. The optimized conformations of WT and p.V240M HCN4 were compared on PyMOL (Molecular Graphics System, Version 2.0 Schrödinger, LLC).

Statistical Analysis. Clinical and experimental results are expressed as mean[SD] and mean ± SEM, respectively. Small-sized samples were first analyzed to determine the distribution of the variables (Normality) using the Shapiro–Wilk and Kolmogorov–Smirnov tests. When these tests demonstrated a normal distribution, parametric tests were used. The paired or unpaired *t* test or one-way ANOVA followed by Tukey's test was used to assess statistical significance where appropriate. When a statistically significant difference was determined by these tests, a Pearson correlation was performed to confirm that the observed differences were not due to random sampling. To make comparisons between fits of pooled or of concentration-dependent data, an F-test was used. To take into account repeated sample assessments, data were analyzed with multilevel mixed-effects models. Variance was similar between groups that were being statistically compared by Student *t* tests or ANOVA tests. A value of $P < 0.05$ was considered significant. For the different groups of experiments, sample size was chosen empirically according to previous experience in the calculation of experimental variability. No statistical method was used to predetermine sample size. The cellular experiments were not blinded due to the nature of the experimental design and platforms, but all the data were analyzed in an identical manner for all conditions to eliminate possible operator bias.

Data, Materials, and Software Availability. CMR and acute and Holter ECGs recordings will be not available since they are incorporated into the confidential medical record of each participant. All other data are included in the manuscript and/or supporting information.

ACKNOWLEDGMENTS. We thank Adam Hoban and Roberto Núñez for critical revision of the MS and Carlos Gil for his excellent technical assistance. This work was funded by Ministerio de Ciencia e Innovación (PID2020–118694RB–I00); Comunidad Autónoma de Madrid (P2022/BMD–7229), European Structural and Investment Funds; and Instituto de Salud Carlos III (CIBERCV; CB16/11/00303).

Author affiliations: [a]Department of Pharmacology and Toxicology, School of Medicine, Universidad Complutense de Madrid, Instituto de Investigación Gregorio Marañón, 28040 Madrid, Spain; [b]Centro de Investigación Biomédica en Red Enfermedades Cardiovasculares, Instituto de Salud Carlos III, Madrid 28029, Spain; [c]Department of Pediatric Cardiology, Virgen de las Nieves University Hospital, Granada 18014, Spain; [d]Instituto de Investigación Biosanitaria de Granada, Granada 18014, Spain; [e]Centro Nacional de Investigaciones Cardiovasculares, Madrid 28029, Spain; and [f]Health in Code Sociedad Limitada, A Coruña 15008, Spain

Author contributions: R.C., J.J.-J., and E.D. designed research; A.C.-C., F.P., M.R.-A., M.D., T.C.-G., J.R., M.M., J.C., R.G., F.B.-J., L.M., J.T., R.C., J.J.-J., and E.D. performed research; A.C.-C., F.P., M.R.-A., M.D., T.C.-G., J.R., M.M., J.C., R.G., F.B.-J., L.M., R.C., J.J.-J., and E.D. analyzed data; and R.C. and E.D. wrote the paper.

1. B. Olshansky, R. M. Sullivan, Inappropriate sinus tachycardia. *Europace* **21**, 194–207 (2019).
2. M. Baruscotti, E. Bianco, A. Bucchi, D. DiFrancesco, Current understanding of the pathophysiological mechanisms responsible for inappropriate sinus tachycardia: Role of the If "funny" current. *J. Interv. Card. Electrophysiol.* **46**, 19–28 (2016).
3. V. C. Nwazue *et al.*, Postural tachycardia syndrome and inappropriate sinus tachycardia: Role of autonomic modulation and sinus node automaticity. *J. Am. Heart Assoc.* **3**, e000700 (2014).
4. P. A. Chiale *et al.*, Inappropriate sinus tachycardia may be related to an immunologic disorder involving cardiac beta adrenergic receptors. *Heart Rhythm* **3**, 1182–1186 (2006).
5. M. Biel, C. Wahl-Schott, S. Michalakis, X. Zong, Hyperpolarization-activated cation channels: From genes to function. *Physiol. Rev.* **89**, 847–885 (2009).
6. D. DiFrancesco, The role of the funny current in pacemaker activity. *Circ. Res.* **106**, 434–446 (2010).
7. I. Rivolta, A. Binda, A. Masi, J. C. DiFrancesco, Cardiac and neuronal HCN channelopathies. *Pflugers Arch.* **472**, 931–951 (2020).
8. K. Hennis, M. Biel, S. Fenske, C. Wahl-Schott, Paradigm shift: New concepts for HCN4 function in cardiac pacemaking. *Pflugers Arch.* **474**, 649–663 (2022).
9. C.-H. Lee, R. MacKinnon, Structures of the human HCN1 hyperpolarization-activated channel. *Cell* **168**, 111–120.e11 (2017).
10. D. DiFrancesco, P. Tortora, Direct activation of cardiac pacemaker channels by intracellular cyclic AMP. *Nature* **351**, 145–147 (1991).
11. B. J. Wainger, M. DeGennaro, B. Santoro, S. A. Siegelbaum, G. R. Tibbs, Molecular mechanism of cAMP modulation of HCN pacemaker channels. *Nature* **411**, 805–810 (2001).
12. A. Porro *et al.*, The HCN domain couples voltage gating and cAMP response in hyperpolarization-activated cyclic nucleotide-gated channels. *eLife* **8**, e49672 (2019).
13. M. Baruscotti, A. Bucchi, D. Difrancesco, Physiology and pharmacology of the cardiac pacemaker ("funny") current. *Pharmacol. Ther.* **107**, 59–79 (2005).
14. W. Shi *et al.*, Distribution and prevalence of hyperpolarization-activated cation channel (HCN) mRNA expression in cardiac tissues. *Circ. Res.* **85**, e1–e6 (1999).
15. N. Li *et al.*, Molecular mapping of sinoatrial node HCN channel expression in the human heart. *Circ. Arrhythm. Electrophysiol.* **8**, 1219–1227 (2015).
16. N. Li *et al.*, Altered microRNA and mRNA profiles during heart failure in the human sinoatrial node. *Sci. Rep.* **11**, 19328 (2021).
17. M. Baruscotti *et al.*, A gain-of-function mutation in the cardiac pacemaker HCN4 channel increasing cAMP sensitivity is associated with familial Inappropriate Sinus Tachycardia. *Eur. Heart J.* **38**, 280–288 (2017).
18. C. H. Peters *et al.*, Isoform-specific regulation of HCN4 channels by a family of endoplasmic reticulum proteins. *Proc. Natl. Acad. Sci. U.S.A.* **117**, 18079–18090 (2020).
19. G. Michels *et al.*, Single-channel properties support a potential contribution of hyperpolarization-activated cyclic nucleotide-gated channels and If to cardiac arrhythmias. *Circulation* **111**, 399–404 (2005).
20. M. C. Brandt *et al.*, Effects of KCNE2 on HCN isoforms: Distinct modulation of membrane expression and single channel properties. *Am. J. Physiol. Heart Circ. Physiol.* **297**, H355–H363 (2009).
21. C. Altomare *et al.*, Integrated allosteric model of voltage gating of HCN channels. *J. Gen. Physiol.* **117**, 519–532 (2001).
22. A. Fabbri, M. Fantini, R. Wilders, S. Severi, Computational analysis of the human sinus node action potential: Model development and effects of mutations. *J. Physiol.* **595**, 2365–2396 (2017).
23. R. Milanesi, M. Baruscotti, T. Gnecchi-Ruscone, D. DiFrancesco, Familial sinus bradycardia associated with a mutation in the cardiac pacemaker channel. *N. Engl. J. Med.* **354**, 151–157 (2006).
24. K. Ueda *et al.*, Functional characterization of a trafficking-defective HCN4 mutation, D553N, associated with cardiac arrhythmia. *J. Biol. Chem.* **279**, 27194–27198 (2004).
25. E. Nof *et al.*, Point mutation in the HCN4 cardiac ion channel pore affecting synthesis, trafficking, and functional expression is associated with familial asymptomatic sinus bradycardia. *Circulation* **116**, 463–470 (2007).
26. V. Macri *et al.*, A novel trafficking-defective HCN4 mutation is associated with early-onset atrial fibrillation. *Heart Rhythm* **11**, 1055–1062 (2014).
27. P. A. Schweizer *et al.*, cAMP sensitivity of HCN pacemaker channels determines basal heart rate but is not critical for autonomic rate control. *Circ. Arrhythm. Electrophysiol.* **3**, 542–552 (2010).
28. A. O. Verkerk, R. Wilders, Pacemaker activity of the human sinoatrial node: An update on the effects of mutations in HCN4 on the hyperpolarization-activated current. *Int. J. Mol. Sci.* **16**, 3071–3094 (2015).
29. M. Cambon-Viala *et al.*, Phenotype/genotype relationship in left ventricular noncompaction: Ion channel gene mutations are associated with preserved left ventricular systolic function and biventricular noncompaction: Phenotype/genotype of noncompaction. *J. Card. Fail.* **27**, 677–681 (2021).
30. M. Alonso-Fernández-Gatta *et al.*, A rare HCN4 variant with combined sinus bradycardia, left atrial dilatation, and hypertrabeculation/left ventricular noncompaction phenotype. *Rev. Española Cardiol. Engl. Ed* **74**, 781–789 (2021).
31. P. A. Schweizer *et al.*, The symptom complex of familial sinus node dysfunction and myocardial noncompaction is associated with mutations in the HCN4 channel. *J. Am. Coll. Cardiol.* **64**, 757–767 (2014).
32. A. Milano *et al.*, HCN4 mutations in multiple families with bradycardia and left ventricular noncompaction cardiomyopathy. *J. Am. Coll. Cardiol.* **64**, 745–756 (2014).
33. H. Yu *et al.*, Contribution of HCN1 variant to sinus bradycardia: A case report. *J. Arrhythmia* **37**, 1337–1347 (2021).
34. A. Refisch *et al.*, A common variation in HCN1 is associated with heart rate variability in schizophrenia. *Schizophr. Res.* **229**, 73–79 (2021).
35. J.-T. He, X.-Y. Li, X. Zhao, X. Liu, Hyperpolarization-activated and cyclic nucleotide-gated channel proteins as emerging new targets in neuropathic pain. *Rev. Neurosci.* **30**, 639–649 (2019).
36. J. C. DiFrancesco *et al.*, HCN ion channels and accessory proteins in epilepsy: Genetic analysis of a large cohort of patients and review of the literature. *Epilepsy Res.* **153**, 49–58 (2019).
37. Z.-J. Wang, I. Blanco, S. Hayoz, T. I. Brelidze, The HCN domain is required for HCN channel cell-surface expression and couples voltage- and cAMP-dependent gating mechanisms. *J. Biol. Chem.* **295**, 8164–8173 (2020).
38. R. S. Sheldon *et al.*, 2015 heart rhythm society expert consensus statement on the diagnosis and treatment of postural tachycardia syndrome, inappropriate sinus tachycardia, and vasovagal syncope. *Heart Rhythm* **12**, e41–e63 (2015).
39. E. Romeo *et al.*, A pediatric case of cardiomyopathy induced by inappropriate sinus tachycardia: Efficacy of ivabradine. *Pediatr. Cardiol.* **32**, 842–845 (2011).
40. P.-F. Winum, G. Cayla, M. Rubini, L. Beck, P. Messner-Pellenc, A case of cardiomyopathy induced by inappropriate sinus tachycardia and cured by ivabradine. *Pacing Clin. Electrophysiol.* **32**, 942–944 (2009).
41. R. Cappato *et al.*, Clinical efficacy of ivabradine in patients with inappropriate sinus tachycardia: A prospective, randomized, placebo-controlled, double-blind, crossover evaluation. *J. Am. Coll. Cardiol.* **60**, 1323–1329 (2012).
42. J. Benezet-Mazuecos *et al.*, Long-term outcomes of ivabradine in inappropriate sinus tachycardia patients: Appropriate efficacy or inappropriate patients. *Pacing Clin. Electrophysiol.* **36**, 830–836 (2013).

43. R. Caballero *et al.*, Tbx20 controls the expression of the *KCNH2* gene and of hERG channels. *Proc. Natl. Acad. Sci. U.S.A.* **114**, E416–E425 (2017).
44. P. Nieto-Marín *et al.*, Tbx5 variants disrupt Nav1.5 function differently in patients diagnosed with Brugada or Long QT Syndrome. *Cardiovasc. Res.* **118**, 1046–1060 (2022).
45. S. Richards *et al.*, Standards and guidelines for the interpretation of sequence variants: A joint consensus recommendation of the American College of Medical Genetics and Genomics and the Association for Molecular Pathology. *Genet Med.* **17**, 405–424 (2015).
46. R. Caballero *et al.*, Flecainide increases Kir2.1 currents by interacting with cysteine 311, decreasing the polyamine-induced rectification. *Proc. Natl. Acad. Sci. U.S.A.* **107**, 15631–15636 (2010).
47. N. Duhme *et al.*, Altered HCN4 channel C-linker interaction is associated with familial tachycardia–bradycardia syndrome and atrial fibrillation. *Eur. Heart J.* **34**, 2768–2775 (2013).
48. A. Bucchi, A. Tognati, R. Milanesi, M. Baruscotti, D. DiFrancesco, Properties of ivabradine-induced block of HCN1 and HCN4 pacemaker channels. *J. Physiol.* **572**, 335–346 (2006).
49. D. Ponce-Balbuena *et al.*, Cardiac Kir2.1 and $Na_V1.5$ Channels Traffic Together to the Sarcolemma to Control Excitability. *Circ. Res.* **122**, 1501–1516 (2018).
50. J. Schymkowitz *et al.*, The FoldX web server: An online force field. *Nucleic Acids Res.* **33**, W382–W388 (2005).